Biotechnology and Bioprocess Engineering
https://doi.org/10.1007/s12257-025-00255-1

RESEARCH PAPER

Efficient production of optically pure (2*S*,3*S*)-butanediol in *Saccharomyces cerevisiae*

Seokjun Moon[1] · Seungwoo Cha[1,2] · Minyoung Kim[3,4] · Changmin Sung[3] · Ji-Sook Hahn[1,2,4]

Received: 17 October 2025 / Revised: 18 December 2025 / Accepted: 24 December 2025

Abstract

(2*S*,3*S*)-Butanediol (BDO) is a valuable chiral diol with growing applications in pharmaceuticals and agriculture, but microbial production is hindered by inefficient (*S*)-acetoin production. Here, we engineered *Saccharomyces cerevisiae* to synthesize (2*S*,3*S*)-BDO directly from glucose by using an efficient (*S*)-acetoin-producing strain, which was generated by introducing *Bacillus subtilis* genes encoding α-acetolactate synthase (*Bs*.AlsS) and a mutant α-acetolactate decarboxylase (*Bs*.AlsD^{WP}) with reversed stereospecificity toward (*S*)-acetoin formation, alongside targeted deletions of genes involved in racemic acetoin production and competing pathways. (2*S*,3*S*)-BDO production in this strain was enabled by introducing *Cg.butA* from *Corynebacterium glutamicum*, encoding an L-butanediol dehydrogenase that reduced (*S*)-acetoin to (2*S*,3*S*)-BDO with high efficiency and stereospecificity. The engineered genome-integrated strains co-expressing *Bs.alsS*, *Bs.alsD*^{WP}, and *Cg.butA* produced 27.9 g/L (2*S*,3*S*)-BDO in fed-batch fermentation with high optical purity, an overall yield of 0.20 g/g glucose, and an average volumetric productivity of 0.17 g/L·h. This represents the first demonstration of high-purity (2*S*,3*S*)-BDO biosynthesis directly from glucose without relying on spontaneous diacetyl-formation pathway, positioning *S. cerevisiae* as a versatile platform for stereoselective diol production.

Keywords (2*S*,3*S*)-butanediol · *Saccharomyces cerevisiae* · Stereoselectivity · L-butanediol dehydrogenase · (*S*)-acetoin

1 Introduction

2,3-Butanediol (2,3-BDO) is a versatile platform chemical with a broad range of industrial and biological applications. It serves as a key precursor for the synthesis of methyl ethyl ketone and 1,3-butadiene—essential intermediates in the production of synthetic rubber and plastics [1]. Additionally, 2,3-BDO is used as a flavoring agent, pharmaceutical intermediate, antifreeze, and a plant growth promoter [2–4]. Due to its two chiral centers, 2,3-BDO exists in three stereoisomeric forms: (2*R*,3*R*)-BDO, *meso*-2,3-BDO, and (2*S*,3*S*)-BDO. The (2*R*,3*R*) isomer is well-studied and widely applied due to its industrial relevance as a chiral building block and precursor for petrochemical derivatives [4]. Its favorable physical properties, such as a low freezing point and high solubility in water, also support its use as an antifreeze and solvent [3, 5]. *meso*-2,3-BDO, although optically inactive, is used in cosmetics and various industrial formulations and has shown moderate antimicrobial activity [6]. In contrast, (2*S*,3*S*)-BDO has received limited attention compared to its other isomers. However, emerging evidence suggests that it exhibits distinct and potentially valuable biological activities. Like the (2*R*,3*R*) isomer, (2*S*,3*S*)-BDO is optically active, and possesses desirable physicochemical traits such as low freezing point and potential as a chiral building block [7]. Moreover, recent studies have demonstrated its ability to suppress the virulence of plant pathogenic bacteria, such as *Ralstonia solanacearum*, a major causative agent of bacterial wilt [8]. Despite the promising applications of these stereoisomers in pharmaceutical, agricultural, and chemical

Seokjun Moon and Seungwoo Cha have contributed equally to this work.

✉ Ji-Sook Hahn
hahnjs@snu.ac.kr

1 Department of Chemical and Biological Engineering, Seoul National University, Seoul 08826, Korea

2 Institute of Chemical Processes, Seoul National University, Seoul 08826, Korea

3 Doping Control Center, Korea Institute of Science and Technology, Seoul 02792, Korea

4 Interdisciplinary Program in Bioengineering, Seoul National University, Seoul 08826, Korea

Published online: 26 January 2026

applications, the selective biosynthesis of enantiomerically pure (2*S*,3*S*)-BDO remains a significant challenge.

Enantiomerically pure 2,3-BDO is conventionally synthesized via petrochemical processes, which have high energy demands and significant environmental impacts. Microbial fermentation has emerged as a more sustainable alternative, utilizing engineered microbial hosts such as *Escherichia coli* [9], *Bacillus subtilis* [10, 11], *Corynebacterium glutamicum* [12], and *Lactococcus lactis* [13] to produce 2,3-BDO from glucose under milder conditions (Table 1). In the canonical 2,3-BDO biosynthetic pathway, pyruvate is initially converted to (*S*)-α-acetolactate by α-acetolactate synthase (ALS). This intermediate is subsequently decarboxylated by α-acetolactate decarboxylase (ALDC) to yield (*R*)-acetoin. The resulting (*R*)-acetoin is then reduced to specific stereoisomers of 2,3-BDO depending on the stereospecificity of the butanediol dehydrogenase (BDH) involved; (2*R*,3*R*)-BDO is produced by D-BDH, whereas *meso*-2,3-BDO is formed by *meso*-BDH [14–16].

However, several bottlenecks remain for the biosynthesis of the (2*S*,3*S*)-BDO. The major challenge is the absence of an efficient enzymatic pathway for (*S*)-acetoin, the key precursor. In the native pathways, (*S*)-α-acetolactate undergoes spontaneous oxidation to diacetyl. Diacetyl is then reduced to (*S*)-acetoin by diacetyl reductase, and further converted to (2*S*,3*S*)-BDO by L-BDH (Fig. 1) [15]. This process involving a non-enzymatic step is inefficient and difficult to control, making it challenging to produce (*S*)-acetoin from glucose alone. A few studies have demonstrated de novo production from glucose using engineered bacteria. Heterologous expression of L-BDH from *Enterobacter cloacae* enabled the production of (2*S*,3*S*)-BDO in both *E. coli* (2.2 g/L) and *L. lactis* (6.7 g/L) [13, 17]. However, these pathways relied on spontaneous non-enzymatic conversion of α-acetolactate to diacetyl, a reaction that required Fe^{3+} supplementation to proceed efficiently. This dependency on spontaneous chemistry and metal ion addition presents a significant limitation for large-scale industrial application.

Another major challenge is the unclear classification and limited characterization of BDHs, which hinders the identification of stereoselective enzymes for (2*S*,3*S*)-BDO production. While D-BDHs have been extensively studied and are typically classified within the medium-chain dehydrogenase/reductase (MDR) family, both L-BDHs and meso-BDHs belong to the short-chain dehydrogenase/reductase (SDR) family and catalyze the formation of the (*S*)-configured hydroxy group [15]. Because they share the same SDR fold, conserved cofactor-binding motifs, and overlapping substrate preferences, enzymes have often been ambiguously annotated or interchangeably referred to as *meso*-BDH or L-BDH. In general, L-BDHs exhibit higher activity toward (*S*)-acetoin, producing (2*S*,3*S*)-BDO, whereas *meso*-BDHs primarily catalyze the conversion of (*R*)-acetoin to *meso*-BDO. However, biochemical characterizations have revealed that certain *meso*-BDHs also reduce (*S*)-acetoin to (2*S*,3*S*)-BDO, and the relative activity toward this substrate varies substantially across species [18]. This ambiguity is further compounded by the fact that certain microorganisms, such as *Klebsiella pneumoniae*, harbor both L-BDH and *meso*-BDH enzymes with partially overlapping activities [15, 19], making it difficult to isolate enzymes with strict stereoselectivity toward (2*S*,3*S*)-BDO. The lack of robust biochemical datasets and clear sequence–function relationships for SDR-type BDHs continues to

Table 1 Microbial enantiomerically pure 2,3-butanediol (BDO) production from glucose

Species	Strategies	Titer (g/L)	Yield (g/g)	Productivity (g/L·h)	Reference
(2*R*,3*R*)-BDO					
Komagataella phaffii (*Pichia pastoris*)	Overexpression of *alsS and alsD* (from *B. subtilis*), *bdh1 (from S. cerevisiae)*	74.5	0.3	0.81	[4]
Corynebacterium glutamicum	Δ*pta* Δ*ack* Δ*ldh* Δ*buta* Δ*nagD* Δ*ppc,* overexpression of *bdhA* (from *B. subtilis*), *udhA* (*from E. coli*)	144.9	0.429	1.10	[12]
Saccharomyces cerevisiae	Δ*adh1* Δ*adh2* Δ*adh3* Δ*adh4* Δ*adh,* Δ*gpd1* Δ*gpd2*, overexpression of *alsS and alsD* (from *B. subtilis*), *noxE* (from *L. lactis*) and endogenous *bdh1*. Fed-batch	72.9	0.41	1.43	[20]
***meso*-BDO**					
Bacillus subtilis	Δ*upp* Δ*acoA* Δ*bdhA* Δ*pta* Δ*ldh*; overexpression of endogenous *alsS, alsD* and *udhA*, *budC* (from *Klebsiella pneumoniae*). Fed-batch	103.7	0.49	0.46	[10]
Bacillus licheniformis	Δ*gdh* Δ*acoR*	98	0.40	0.94	[16]
(2*S*,3*S*)-BDO					
Lactococcus lactis	Δ*ldh* Δ*pta* Δ*adhE* Δ*aldB* Δ*butBA* Δ*noxE*, overexpression of *budC* (from *Enterobacter cloacae*). hemin/Fe^{3+}-driven (*S*)-α-acetolactate decarboxylation	6.7	0.41	0.082	[13]
Escherichia coli	Overexpression of *budB* and *budC* (from *E. cloacae*). Fe^{3+}-driven (*S*)-α-acetolactate decarboxylation	2.2	0.08	0.09	[17]
S. cerevisiae	*bdh1*Δ *pdc1*Δ *pdc5*Δ *ora1*Δ *adh1*Δ *gpd1*Δ overexpression of *alsS, alsD*^{WP} (from *B. subtilis*), *butA* (from *C. glutamicum*)	27.9	0.20	0.17	This study

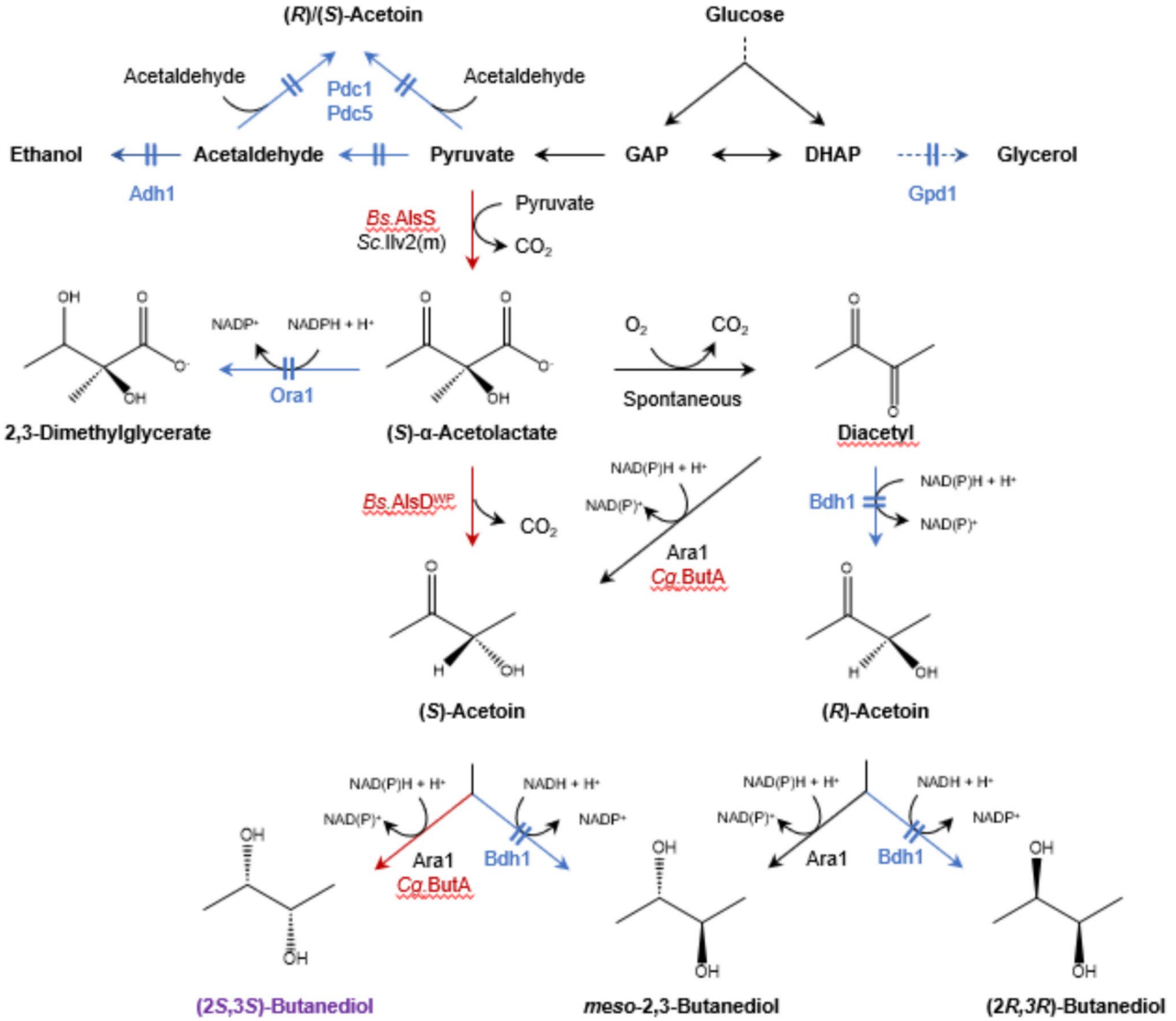

Fig. 1 Schematic representation of the biosynthetic pathway for (2*S*,3*S*)-BDO production. Genes involved in the native pathway are shown in black, heterologous genes in red, and deleted genes in blue. The pathway illustrates key steps for (2*S*,3*S*)-BDO production, including the introduction of heterologous genes for intermediate conversions and the deletion of competing pathways to enhance production efficiency. BDO: butanediol

impede the rational screening and engineering of stereospecific catalysts for chiral 2,3-BDO biosynthesis.

Saccharomyces cerevisiae is a GRAS organism with strong industrial potential. Owing to its inherently high glycolytic flux and subsequent pyruvate accumulation, it has been engineered for the production of various pyruvate-derived compounds including 2,3-BDO [20], acetoin [21–23], and lactic acid [24, 25]. Previously, we achieved 72.9 g/L of (2*R*,3*R*)-BDO [20] and 101.3 g/L of (*R*)-acetoin [21] by introducing a heterologous pathway, ALS (*Bs*.AlsS) and ALDC (*Bs*.AlsD) from *B. subtilis*, to convert pyruvate into (*R*)-acetoin, alongside optimization of key metabolic pathways [26]. *S. cerevisiae* also harbors other dehydrogenases, Ara1, Ora1, and Ypr1 [21, 27, 28], that have been shown to exhibit the activity of converting (*S*)-acetoin to (2*S*,3*S*)-BDO in vitro [21]. However, because these enzymes exhibit broad substrate specificity and participate in multiple native pathways beyond 2,3-BDO biosynthesis, their suitability for selective (2*S*,3*S*)-BDO production is limited.

Recently, we engineered a mutant *Bs*.AlsD$^{M154W\ E251P}$ (*Bs*.AlsD^{WP}), which alters the enzyme's stereoselectivity to favor the production of (*S*)-acetoin over the native (*R*)-form from (*S*)-α-acetolactate [22]. When expressed in *S. cerevisiae*, together with deletion of *PDC1* and *PDC5*, encoding pyruvate decarboxylase to eliminate endogenous racemic acetoin formation, this engineered pathway enabled the

Table 2 Stepwise strategies to improve (2*S*,3*S*)-BDO production in *S. cerevisiae*

Step	Strategy	Description	Medium	Titer (g/L)
1	Base strain	(*S*)-acetoin-producing base strain (JHYA203-3D)	2% SC	0.23
2	L-BDH screening	Selection of *Cg*.ButA	2% SC	1.04
3	Pathway expression optimization	Promoter replacement and genomic integration of (2*S*,3*S*)-BDO pathway genes (JHYA301)	2% SC	2.13
4	Medium optimization	Selection of 5% YPD as the cultivation medium	5% YPD	3.71
5	Flask fed-batch	100 mL flask fed-batch cultivation	5% YPD	16.53
6	Fermenter fed-batch	1 L fermenter fed-batch cultivation	5% YPD	27.9

BDO: butanediol, BDH: butanediol dehydrogenase, SC: synthetic complete

Table 3 Strains used in this study

Strain	Genotype	Reference
CEN.PK2-1C	*MATa ura3-52 trp1-289 leu2-3,112 his3Δ1 MAL2-8C SUC2*	EUROSCARF
JHYA203	*bdh1*Δ *pdc1*Δ *pdc5*Δ *ora1*Δ *adh1*Δ *gpd1*Δ	[22]
JHYA203-D	JHYA203 H8::P_{TDH3}-*Bs.alsD*^{WP}-T_{CYC1}	This study
JHYA203-2D	JHYA203-D H2::P_{TDH3}-*Bs.alsD*^{WP}-T_{CYC1}	This study
JHYA203-3D	JHYA203-2D H4::P_{TDH3}-*Bs.alsD*^{WP}-T_{CYC1}	This study
JHYA300	JHYA203-3D H6::P_{TDH3}-*Cg.butA*-T_{CYC1}	This study
JHYA301	JHYA300 H1::P_{TDH3}-*Bs.alsS*-T_{CYC1}	This study

de novo production of high-purity (*S*)-acetoin (723 mg/L) directly from glucose, without the need for chemical additives to induce spontaneous diacetyl formation.

In this study, we engineered *S. cerevisiae* to produce (2*S*,3*S*)-BDO de novo from glucose based on this newly developed (*S*)-acetoin pathway (Table 2). Fed-batch fermentation in a 1 L bioreactor produced 27.9 g/L of (2*S*,3*S*)-BDO with an overall yield of 0.20 g/g glucose and average volumetric productivity of 0.17 g/L/h, representing the highest reported titer of optically pure (2*S*,3*S*)-BDO to date and the first achieved without full reliance on diacetyl, which typically requires precursor supplementation or chemical additives to promote spontaneous conversion.

2 Materials and methods

2.1 Strains and culture conditions

All strains used in this study are listed in Table 3. Strain construction was carried out using the CRISPR/Cas9-mediated genome editing system as previously described [22]. Gene expression cassettes were integrated into the H1, H2, H4, H6, and H8 neutral loci using backbone vectors containing homology arms. Transformants were selected on synthetic complete (SC) medium lacking the appropriate amino acids.

Yeast cells harboring the appropriate plasmids were first pre-cultured in 5 mL of SC medium (6.7 g/L yeast nitrogen base without amino acids and 1.4 g/L amino acid dropout mixture lacking His, Trp, Leu, and Ura) supplemented with the appropriate amino acids in 50 mL Erlenmeyer flasks. After overnight culture, the cells were diluted to an initial OD_{600} of 0.2 in 10 mL of the same medium and cultivated in 100 mL Erlenmeyer flasks at 30 °C with shaking at 170 rpm. After genome integration, batch cultures in Erlenmeyer flasks were performed using either complete SC medium or YPD medium (10 g/L yeast extract and 20 g/L bacto-peptone), each supplemented with 20 g/L or 50 g/L glucose, under the same cultivation conditions.

Fed-batch fermentation was performed using a 1 L benchtop fermenter (FMT-DS, Fermentec) containing 500 mL of YPD medium with 50 g/L glucose. The culture was maintained at 30 °C with an agitation speed of 550 rpm and an aeration rate of 1.0 vvm. *S. cerevisiae* strain JHYA301 was pre-cultured overnight in YPD medium containing 50 g/L glucose, and 10 mL of this pre-culture was used to inoculate 490 mL of fresh YPD medium. Based on the estimated glucose consumption rate, 50 mL of concentrated glucose solution (500 g/L) was intermittently added every 12 or 24 h, thereby increasing the glucose concentration by approximately 50 g/L at each feeding.

2.2 Construction of plasmids

The sequence of bacterial genes used in this study is listed in Table S1. *Bs.alsS* and mutant *Bs.alsD*^{WP} genes were used as previously described [22]. In addition, *l-bdh* genes derived from *Corynebacterium glutamicum* (*Cg.butA*), *Rhodococcus erythropolis* (*Re.dar*), and *K. pneumoniae* (*Kp.ardII*), each codon-optimized for *S. cerevisiae*, were cloned into the p416G expression plasmid [29] using *Bcu*I and *Xho*I restriction sites for functional characterization, whereas *S. cerevisiae ara1* was cloned using *Xba*I and *Xho*I. For genomic integration of selected genes including *Bs.alsS*, *Bs.alsD*^{WP}, and *Cg.butA*, expression cassettes were PCR-amplified using primers containing *Mau*BI and *Not*I restriction sites and cloned into donor vectors targeting neutral loci (H1, H2,

H4, H6, or H8). The resulting donor plasmids were used for CRISPR/Cas9-mediated integration into the *S. cerevisiae* genome. A full list of plasmids and primers used in this study is provided in Table 4 and Table S2.

2.3 In vitro enzyme assay

His_6-tagged *Cg*.ButA enzymes were purified from *E. coli* Rosetta-gami2 (DE3) pLysS using a previously described method [21, 22]. For enzymatic assays, a total reaction volume of 200 µL was prepared containing 10 µM of purified protein, 5 mM acetoin, 5 mM NADPH, and 10 mM sodium phosphate buffer (pH 7.0). The mixture was incubated at 25 °C for 16 h to allow extensive conversion of acetoin prior to extraction. Following the reaction, 2,3-BDO was extracted using a salting-out method by dissolving dipotassium phosphate (K_2HPO_4) to a final concentration of 60% (w/v), followed by the addition of ethyl acetate at twice the reaction volume. The extracted product was analyzed by

Table 4 Plasmids used in this study

Plasmid	Description	Reference
Plasmids for gene expression		
p413G	CEN/ARS plasmid, *HIS3*, P_{TDH3}, T_{CYC1}	[29]
p414G	CEN/ARS plasmid, *TRP1*, P_{TDH3}, T_{CYC1}	[29]
p416G	CEN/ARS plasmid, *URA3*, P_{TDH3}, T_{CYC1}	[29]
p413A	CEN/ARS plasmid, *HIS3*, P_{ADH1}, T_{CYC1}	[29]
p413G-*alsS*	CEN/ARS plasmid, *HIS3*, P_{TDH3}-*Bs.alsS*-T_{CYC1}	[22]
p413A-*alsS*	CEN/ARS plasmid, *HIS3*, P_{ADH1}-*Bs.alsS*-T_{CYC1}	[22]
p414G-$alsD^{WP}$	CEN/ARS plasmid, *TRP1*, P_{TDH3}-*Bs.alsD*^{WP}-T_{CYC1}	[22]
p416G-*ara1*	CEN/ARS plasmid, *URA3*, P_{TDH3}-*ara1*-T_{CYC1}	This study
p416G-*Cg.butA*	CEN/ARS plasmid, *URA3*, P_{TDH3}-*Cg.butA*-T_{CYC1}	This study
p416G-*Re.dar*	CEN/ARS plasmid, *URA3*, P_{TDH3}-*Re.dar*-T_{CYC1}	This study
p416G-*Kp.ardII*	CEN/ARS plasmid, *URA3*, P_{TDH3}-*Kp.ardII*-T_{CYC1}	This study
Plasmids for genomic integration		
Coex415-Cas9	CEN/ARS plasmid, *LEU2*, P_{TDH3}-Cas9-T_{TPI1}	This study
p426-H1gRNA	2µ plasmid, *URA3*, P_{SNR52}-H1 gRNA-T_{SUP4}	This study
p426-H6gRNA	2µ plasmid, *URA3*, P_{SNR52}-H6 gRNA-T_{SUP4}	This study
Coex416-Cas9-H2gRNA	CEN/ARS plasmid, *URA3*, P_{TDH3}-Cas9-T_{TPI1}, P_{SNR52}-H2 gRNA-T_{SUP4}	This study
Coex416-Cas9-H4gRNA	CEN/ARS plasmid, *URA3*, P_{TDH3}-Cas9-T_{TPI1}, P_{SNR52}-H4 gRNA-T_{SUP4}	This study
Coex416-Cas9-H8gRNA	CEN/ARS plasmid, *URA3*, P_{TDH3}-Cas9-T_{TPI1}, P_{SNR52}-H8 gRNA-T_{SUP4}	This study
pInt_H1	H1 site integration plasmid containing H1 upstream and downstream	This study
pInt_H1-*alsS*	Plasmid containing P_{TDH3}-*Bs.alsS*-T_{CYC1} flanked by H1 upstream and downstream	This study
pInt_H2	H2 site integration plasmid containing H2 upstream and downstream	This study
pInt_H2-$alsD^{WP}$	Plasmid containing P_{TDH3}-*Bs.alsD*^{WP}-T_{CYC1} flanked by H2 upstream and downstream	This study
pInt_H4	H4 site integration plasmid containing H4 upstream and downstream	This study
pInt_H4-$alsD^{WP}$	Plasmid containing P_{TDH3}-*Bs.alsD*^{WP}-T_{CYC1} flanked by H4 upstream and downstream	This study
pInt_H8	H8 site integration plasmid containing H8 upstream and downstream	This study
pInt_H8-$alsD^{WP}$	Plasmid containing P_{TDH3}-*Bs.alsD*^{WP}-T_{CYC1} flanked by H8 upstream and downstream	This study
pInt_H6	H6 site integration plasmid containing H6 upstream and downstream	This study
pInt_H6-*Cg.butA*	Plasmid containing P_{TDH3}-*Cg.butA*-T_{CYC1} flanked by H6 upstream and downstream	This study
Plasmids used in enzyme assay		
pET-28b(+)	Kan^R, His_6-tagged protein expression vector	Novagen
pET-*Cg.butA*	*Cg.butA*-His_6 expression plasmid	This study

gas chromatography-mass spectrometry (GC–MS) to determine the stereoisomeric composition of 2,3-BDO.

2.4 Molecular docking simulation

Molecular docking simulations were performed using AutoDock Vina v1.2.7 [30, 31]. The crystal structures of L-BDH from *C. glutamicum* (PDB ID: 3A28) [32] and *meso*-BDH from *K. pneumoniae* (PDB ID: 1GEG) [33] were obtained from the Protein Data Bank. The structures of (*S*)-acetoin (PubChem CID: 447765) and (*R*)-acetoin (PubChem CID: 439314) were used as ligands. All molecules were preprocessed using UCSF Chimera [34] for hydrogen addition and format conversion. Docking poses were ranked by predicted binding affinity, and the final pose was selected based on both the docking score and visual inspection of the binding conformation at the active site.

2.5 Analytical methods

Cell growth and metabolite analysis were conducted as previously reported [22], with no modifications. Briefly, OD_{600} was measured to monitor cell growth, and culture supernatants were analyzed by HPLC using a BioRad Aminex HPX-87H column and RI detector under standard conditions (5 mM H_2SO_4, 60 °C column, 35 °C detector).

For GC–MS analysis, samples were analyzed by Agilent Technologies 7890B GC and 5977A MSD system equipped with a β-DEX™ 120 column (30 m × 0.25 mm × 0.25 µm film thickness, Supelco). Nitrogen was used as the carrier gas. The initial GC oven temperature was programmed from 65 °C for 3 min and then was linearly ramped up to 100 °C at 2 °C/min (held for 5 min). The total run time was 25.5 min. The injector and the GC–MS transfer lines were set at 230 °C. The injection volume was 1 µL, and the split ratio was set to 5:1. Target peaks were extracted by merging extracted ion chromatograms at m/z 45, 57, and 71. Retention times of (2*S*,3*S*)-BDO, (2*R*,3*R*)-BDO and *meso*-2,3-BDO were 15.1 min, 15.5 min and 16.5 min, respectively. Acquired data were evaluated with Agilent MassHunter Qualitative Analysis software (Version 10.0) for peak shape, retention time, and MS spectrum [35].

3 Results

3.1 Strain engineering to produce (2*S*,3*S*)-BDO

Since (2*S*,3*S*)-BDO is produced from (*S*)-acetoin by L-BDH, increasing the level of (*S*)-acetoin is essential for (2*S*,3*S*)-BDO production (Fig. 1). Previously, we engineered *Bs*.AlsD^{WP}, a ALDC from *B. subtilis*, with altered stereospecificity to produce (*S*)-acetoin instead of (*R*)-acetoin from (*S*)-α-acetolactate [22]. Given the reduced catalytic activity of this mutant enzyme compared to wild-type *Bs*.AlsD, we integrated three copies of *Bs.alsD*^{WP} into neutral chromosomal loci (H2, H4, and H8) of the previously engineered *S. cerevisiae* strain JHYA203 [22]. The JHYA203 strain *was* constructed by deleting the endogenous racemic acetoin-producing pathway (*pdc1Δ* and *pdc5Δ*), (*R*)-alcohol-specific NADH-dependent 2,3-butanediol dehydrogenase (*bdh1Δ*) and major competing pathways for ethanol (*adh1Δ*), glycerol (*gpd1Δ*), and 2,3-dimethylglycerate (*ora1*Δ) (Fig. 1). The resulting strain, JHYA203-3D, served as the starting platform for (2*S*,3*S*)-BDO production in this study, with the integration of three copies of *Bs.alsD*^{WP} confirmed by qPCR analysis (Fig. S1).

Using the JHYA203-3D, we screened several L-BDH enzymes for (2*S*,3*S*)-BDO production. Among previously reported L-BDH enzymes, three candidates from *C. glutamicum* (*Cg*.ButA), *R. erythropolis* (*Re*.Dar), and *K. pneumoniae* (*Kp*.ArdII) were selected for their proven ability to produce (2*S*,3*S*)-BDO in vivo or in vitro [19, 36, 37]. In addition, we tested *S. cerevisiae*'s endogenous dehydrogenase Ara1, which has been shown to exhibit (*S*)-stereoselective reduction of (*S*)-acetoin to (2*S*,3*S*)-BDO [21].

To evaluate the activity of each enzyme in the JHYA203-3D strain, four L-BDH genes were individually expressed under the strong *TDH3* promoter using the low copy number plasmid vector (p416G) and co-expressed with *Bs.alsS* and *Bs.alsD*^{WP} on separate plasmids (Fig. 2A). We previously observed that strong expression of *Bs.alsS* led to growth defects due to the accumulation of the toxic intermediate (*S*)-α-acetolactate [22, 38]. This compound undergoes spontaneous oxidative decarboxylation to form diacetyl—a highly reactive electrophilic compound. Diacetyl is known to covalently modify cellular proteins, particularly at lysine and cysteine residues, leading to protein dysfunction and growth inhibition [39]. Therefore, *Bs.alsS* was expressed from the weaker *ADH1* promoter on the p413A plasmid. Although *Bs.alsD*^{WP} was already integrated in JHYA203-3D, it was additionally expressed under the *TDH3* promoter via the p414G plasmid to enhance (*S*)-acetoin production. All tested strains showed normal growth without significant defects in SC-HLU medium with 20 g/L glucose (Fig. S2). The control strain carrying an empty p416G plasmid produced 435.5 mg/L (*S*)-acetoin (Fig. 2A). Even without additional L-BDH expression, 230.6 mg/L of (2*S*,3*S*)-BDO was produced, attributable to the activity of endogenous dehydrogenases, such as Ara1, capable of reducing (*S*)-acetoin to (2*S*,3*S*)-BDO (Fig. 2A). Among the enzymes tested, *Cg*.ButA, *Re*.Dar, and *Sc*.Ara1 increased (2*S*,3*S*)-BDO, with *Cg*.ButA showing the highest efficacy, reaching a titer of 1,040 mg/L. In the strain expressing *Cg*.ButA, most of the

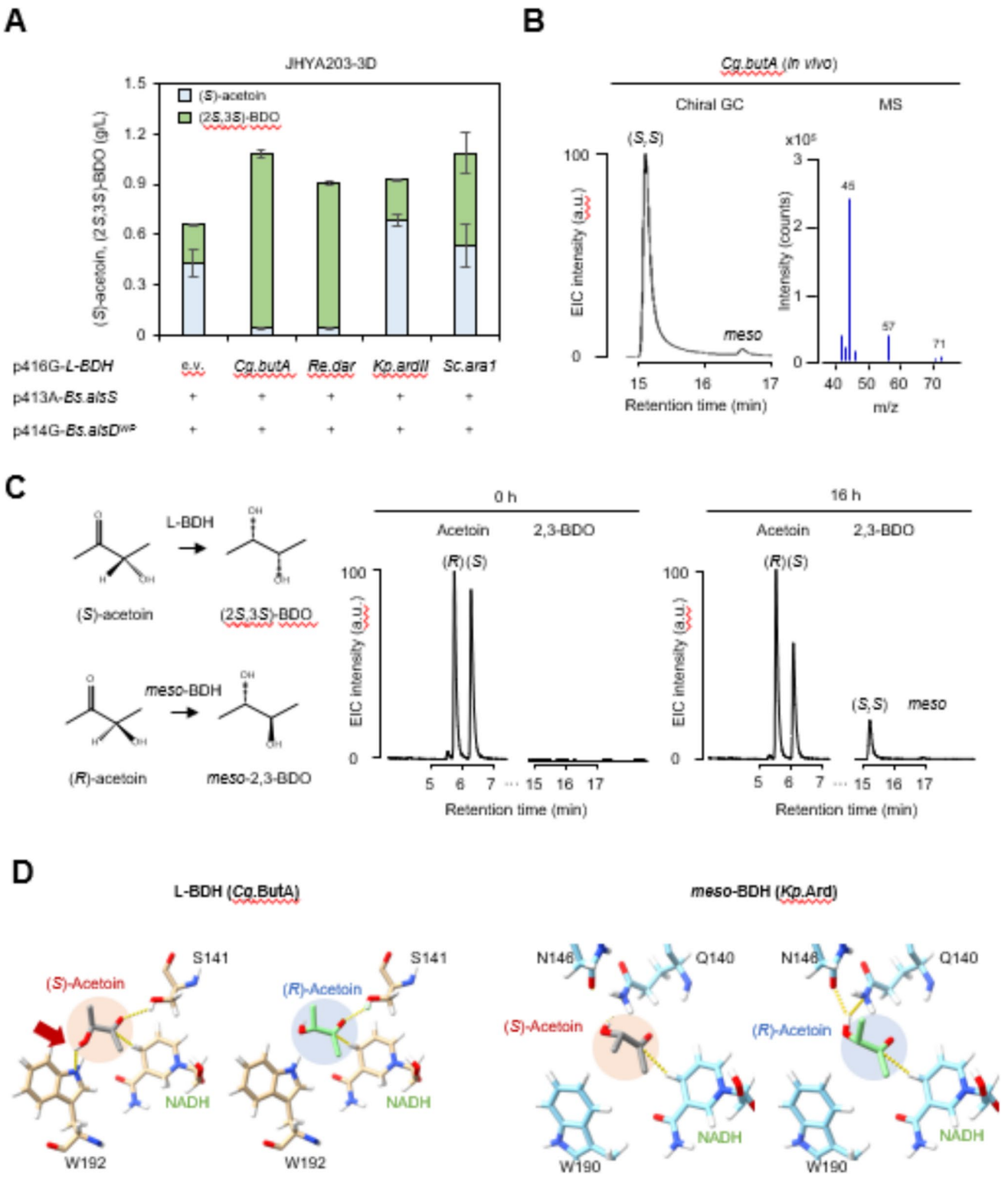

Fig. 2 Screening of L-BDH for (2*S*,3*S*)-BDO production. (**A**) Comparison of (*S*)-acetoin and (2*S*,3*S*)-BDO production in JHYA203-3D strains harboring p416G-L-BDH (expressing different L-BDH candidates) together with p413A-*alsS* and p414G-*alsD*^{WP}. Cells were grown in SC-HLU medium with 20 g/L glucose for 72 h. (**B**) Chiral GC–MS analysis of (2*S*,3*S*)-BDO produced by *Cg.butA* expression, using culture broth collected after 72 h of cultivation, with the left panel showing extracted ion chromatogram (EIC) trace and the right panel showing MS spectra. (**C**) In vitro enzyme assay of purified *Cg*.ButA using a racemic mixture of (*R*)- and (*S*)-acetoin as substrates. (**D**) Molecular docking simulations of L-BDH (*Cg*.ButA) (left) and *meso*-BDH (*Kp*. Ard) (right) with both (*S*)-acetoin and (*R*)-acetoin in the presence of NADH. Key residues are labeled and shown as sticks. Carbon atoms of L-BDH and *meso*-BDH are colored beige and cyan, respectively. BDO: butanediol, BDH: butanediol dehydrogenase, SC: synthetic complete, GC–MS: gas chromatography-mass spectrometry

(*S*)-acetoin was converted to (2*S*,3*S*)-BDO, leaving only 43.5 mg/L of unreacted (*S*)-acetoin. Based on this result, *Cg*.ButA was selected for further characterization.

To verify the stereoisomeric purity of product, chiral GC–MS was performed using standards for all three 2,3-BDO isomers (Fig. S3), clearly confirming that the major product was (2*S*,3*S*)-BDO (Fig. 2B). Only trace amounts of *meso*-2,3-BDO were detected, presumably due to residual formation of (*R*)-acetoin during fermentation, whereas (2*R*,3*R*)-BDO was not detected. To further investigate the stereospecificity of *Cg*.ButA, we performed in vitro enzyme assays using the purified protein and analyzed the reaction products via chiral GC–MS. Racemic acetoin was used as the substrate, from which (*S*)-acetoin is expected to be converted to (2*S*,3*S*)-BDO by L-BDH, while (*R*)-acetoin would yield *meso*-2,3-BDO by *meso*-BDH. As shown in Fig. 2C, after 16 h of reaction, the (*S*)-acetoin peak was markedly decreased with the concomitant production of (2*S*,3*S*)-BDO, whereas (*R*)-acetoin remained largely unreacted. Only trace amounts of *meso*-2,3-BDO were detected, confirming the enzyme's strong preference for the (*S*)-enantiomer, consistent with a previous report demonstrating a 140-fold higher k_{cat}/K_m for (*S*)-acetoin over (*R*)-acetoin by *Cg*.ButA [36].

To investigate the underlying structural basis of the stereospecificity of *Cg*.ButA, we performed molecular docking simulations using AutoDock Vina [30, 31] with the crystal structure of *Cg*.ButA (PDB ID: 3A28) [32] as the receptor (Fig. 2D, left panel). Docking of (*S*)-acetoin revealed stabilization via a hydrogen bond between its chiral hydroxyl group in the indole NH of Trp192, along with polar interactions with Ser141. In contrast, (*R*)-acetoin failed to form a hydrogen bond with Trp192 due to misalignment, despite retaining interaction with Ser141, suggesting weaker stabilization. This finding supports and extends a previous 2-mercaptoethanol-based model [32], highlighting the key role of Trp192, and further reveals a more pronounced stereospecific interaction favoring the (*S*)-acetoin.

To compare with *Cg*.ButA, we also performed docking simulations using the crystal structure of *meso*-BDH (*Kp*.Ard) from *K. pneumoniae* (PDB ID: 1GEG) [33], which exhibits substrate specificity toward the (*R*)-acetoin enantiomer (Fig. 2D, right panel). In the *Kp*.Ard binding pocket, (*R*)-acetoin forms well-aligned hydrogen bonds between its hydroxyl group and the side chains of Asn146 and Gln140, resulting in a highly favorable binding geometry. In contrast, (*S*)-acetoin adopts a tilted conformation that disrupts optimal hydrogen bonding, leading to reduced stabilization. While *Cg*.ButA relies on Trp192 as a critical determinant of stereospecificity, *Kp*.Ard contains the corresponding Trp190 but its indole NH is oriented away from the substrate and does not participate in hydrogen bonding, thereby failing to influence substrate specificity. This structural arrangement accounts for *Kp*.Ard's catalytic bias toward (*R*)-acetoin, in contrast to the selectivity of *Cg*.ButA, thereby highlighting the structural features that govern stereoselectivity in L-BDH enzymes.

Fig. 3 Optimization of strain and media for (2*S*,3*S*)-BDO production. (**A**) (2*S*,3*S*)-BDO production levels depending on *Bs.alsS* expression levels. JHYA203-3D strains harboring p414G-$alsD^{WP}$, p416G-*Cg.butA*, and either p413G-*alsS* (P_{TDH3}-*Bs.alsS*) or p413A-*alsS* (P_{ADH1}-*Bs.alsS*) were grown in SC-HLU medium with 20 g/L glucose. (Left) Growth curves. (Right) Production levels of (*S*)-acetoin and (2*S*,3*S*)-BDO. (**B**) Growth curves and glucose consumption rates of JHYA301 strain grown in YPD medium (left) and SC medium (right) with either 2% or 5% glucose. (**C**) (2*S*,3*S*)-BDO production and chiral GC profiles of JHYA301 in various media. Both (2*S*,3*S*)-BDO titers and chiral GC data were obtained from culture broth collected after 72 h of cultivation. BDO: butanediol, SC: synthetic complete, GC: gas chromatography, EIC: extracted ion chromatogram

3.2 Generation of stable integrative strains

For our initial evaluation, we expressed $Bs.alsD^{WP}$ and *Cg.butA* under the *TDH3* promoter, while *Bs.alsS* was placed under the weaker *ADH1* promoter due to concerns about the toxicity of (*S*)-α-acetolactate. However, we hypothesized that overexpressing $Bs.alsD^{WP}$ and *Cg.butA* might alleviate this toxicity by converting (*S*)-α-acetolactate to (2*S*,3*S*)-BDO. To test this, *Bs.alsS* was also expressed under the strong *TDH3* promoter (p413G-*alsS*), together with p414G-$alsD^{WP}$ and p416G-*Cg.butA* (Fig. 3A). Cells carrying p413G-*alsS* exhibited a growth rate comparable to those with p413A-*alsS*. *Bs.alsS* expression from the *TDH3* promoter raised the (2*S*,3*S*)-BDO titer to 1,192 mg/L, about 20% higher than obtained with the *ADH1* promoter. This indicates that overexpressing *Cg.butA* reduces (*S*)-α-acetolactate toxicity by effectively driving flux toward (2*S*,3*S*)-BDO.

Based on these results, we proceeded with genome integration of P_{TDH3}-*Bs.alsS* to enhance genetic stability. Although direct integration into the JHY203-3D strain was unsuccessful—likely due to residual (*S*)-α-acetolactate toxicity—successful integration was achieved using a sequential strategy. First, P_{TDH3}-*Cg.butA* was integrated into the H6 locus of JHYA203-3D, generating JHYA300. Subsequently, P_{TDH3}-*Bs.alsS* was successfully integrated into the H1 locus of JHYA300, resulting in strain JHYA301, a fully genome-integrated (2*S*,3*S*)-BDO producing strain.

To optimize culture conditions for (2*S*,3*S*)-BDO production, strain JHYA301 was cultivated in SC and YPD media containing either 2% or 5% glucose (Fig. 3B and C). In SC medium with 2% glucose, JHYA301 produced 2.1 g/L (2*S*,3*S*)-BDO (Fig. 3C), surpassing the titer (1.2 g/L) achieved with plasmid-based expression of the biosynthetic genes (Fig. 3A), demonstrating the efficiency of this genome-integrated strain. After 72 h, (2*S*,3*S*)-BDO titers in SC medium were higher than those in YPD at 2% glucose;

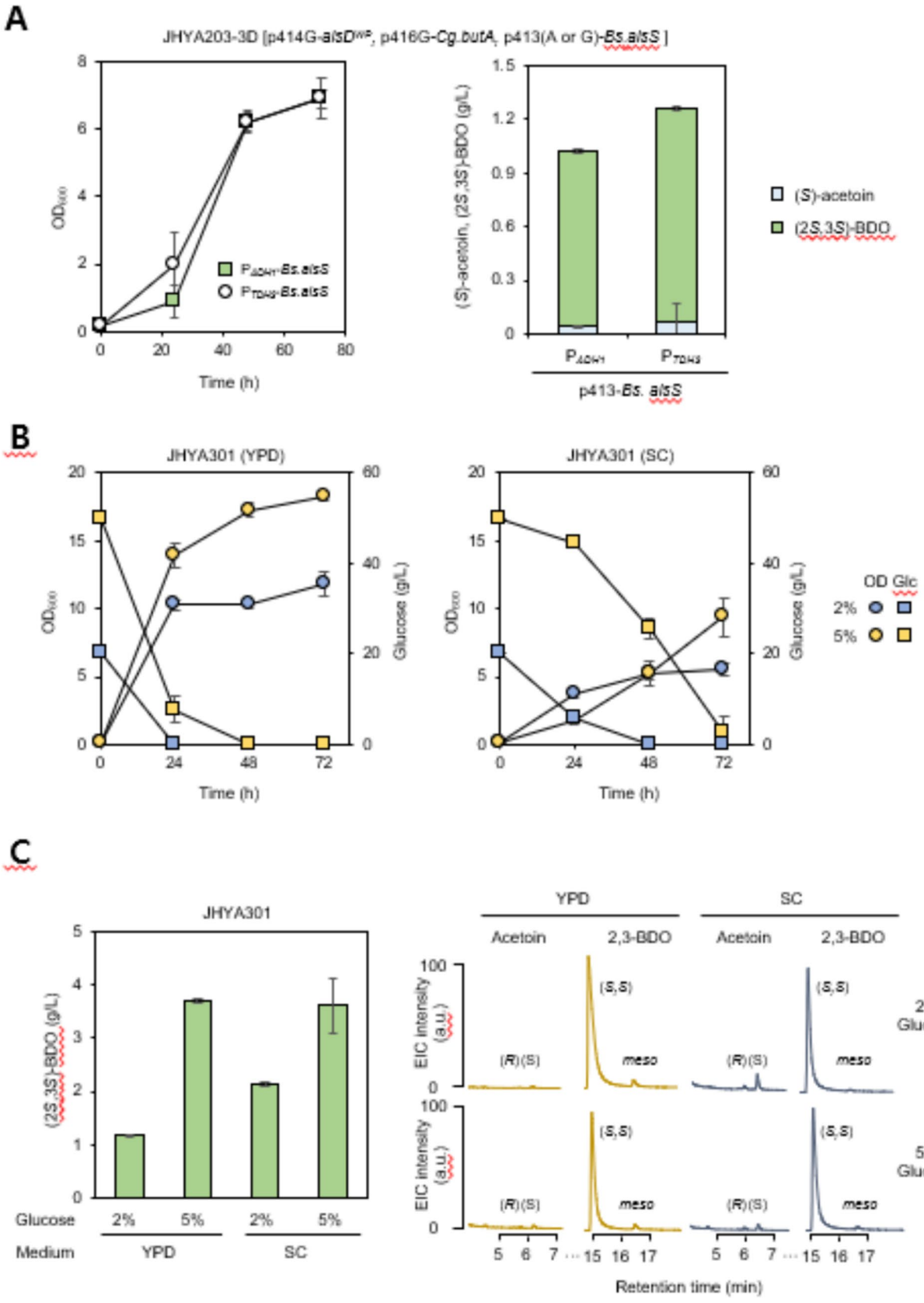
A
JHYA203-3D [p414G-alsD^WP, p416G-Cg.butA, p413(A or G)-Bs.alsS]
OD600
Time (h)
P_ADH1-Bs.alsS
P_TDH3-Bs.alsS
(S)-acetoin, (2S,3S)-BDO (g/L)
(S)-acetoin
(2S,3S)-BDO
p413-Bs. alsS
B
JHYA301 (YPD)
JHYA301 (SC)
Glucose (g/L)
OD Glc
2%
5%
C
JHYA301
(2S,3S)-BDO (g/L)
Glucose
Medium
YPD
SC
Acetoin
2,3-BDO
EIC intensity (a.u.)
(S,S)
(R)(S)
meso
2% Glucose
5% Glucose
Retention time (min)

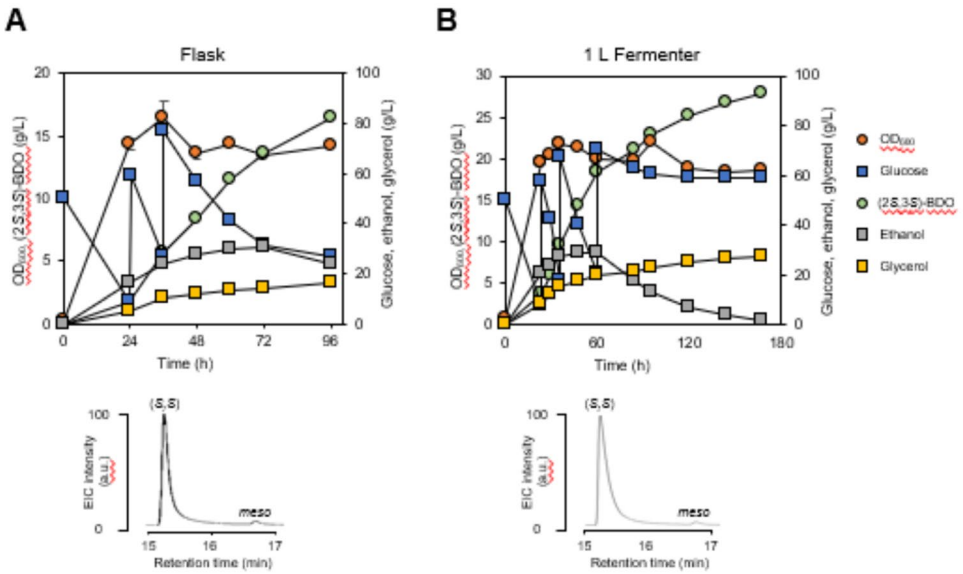

Fig. 4 Fed-batch fermentation for (2*S*,3*S*)-BDO production. (**A**) Flask-scale fed-batch fermentation of the JHYA301 strain showing (2*S*,3*S*)-BDO production (top) and chiral GC analysis of the product (bottom). Chiral GC was performed on culture broth collected at 96 h. (**B**) Fermenter-scale fed-batch fermentation results for (2*S*,3*S*)-BDO production (top) and corresponding chiral GC analysis (bottom). Chiral GC was performed on culture broth collected at 168 h. Cell growth, glucose consumption, and metabolite production were monitored throughout cultivation. BDO: butanediol, GC: gas chromatography, EIC: extracted ion chromatogram

however, under 5% glucose, both media yielded comparable titers. Despite the higher production in SC medium at low glucose concentrations, cells displayed slower growth and markedly reduced glucose consumption in SC compared to YPD. These results indicate that YPD medium is better suited for subsequent fed-batch and scale-up fermentations, where rapid and sustained glucose utilization is critical. Additionally, chiral GC–MS analysis of the fermentation products confirmed efficient conversion of acetoin to 2,3-BDO. The final product exhibited high chiral purity, with (2*S*,3*S*)-BDO accounting for over 97% of stereoselectivity in both 5% YPD and 5% SC media, indicating effective stereoselective conversion and minimal *meso*-2,3-BDO formation under both conditions.

3.3 Increasing (2*S*,3*S*)-BDO production by fed-batch fermentation

To further increase (2*S*,3*S*)-BDO production and evaluate pathway performance under extended cultivation, flask-scale fed-batch fermentation was first performed using the JHYA301 strain. Based on batch culture results (Fig. 3C), 5% YPD was used as the base medium for fed-batch operation. Under these conditions, JHYA301 produced 16.53 g/L of (2*S*,3*S*)-BDO at 96 h (Fig. 4A). GC–MS analysis revealed that (2*S*,3*S*)-BDO was the major product, while *meso*-2,3-BDO was detected only at negligible levels.

Based on these promising flask-scale results, particularly the low byproduct levels, we scaled up the process using a 1 L bioreactor system. After 168 h of cultivation, JHYA301 produced 27.9 g/L of (2*S*,3*S*)-BDO with high enantiomeric purity, while *meso*-2,3-BDO was detected only at trace levels (Fig. 4B). The overall yield and average volumetric productivity in this fed-batch process were 0.20 g/g glucose and 0.17 g/L·h, respectively, indicating efficient conversion of glucose to the desired (2*S*,3*S*)-BDO under these conditions. To better understand how carbon was redistributed between product formation and byproduct pathways during fed-batch fermentation, we analyzed the time-course profiles of glucose, ethanol, and (2*S*,3*S*)-BDO in the bioreactor.

In the fed-batch cultivation, ethanol accumulated during the early phase while glucose was still present, reaching approximately 29 g/L, and was subsequently re-consumed after around 60 h when cell growth had ceased and glucose uptake had slowed (Fig. 4B). During this ethanol-consumption period, the (2*S*,3*S*)-BDO concentration continued to increase, indicating that the culture remained metabolically active despite the absence of detectable biomass formation. As a result, a substantial portion of the final (2*S*,3*S*)-BDO titer was produced during the non-growing phase, although the volumetric productivity during this period was considerably lower than during the growth-associated phase.

4 Discussion

Building on our (*S*)-acetoin chassis in *S. cerevisiae* [22], which incorporated the engineered *Bs.alsD*^{WP} mutant to reverse stereospecificity toward (*S*)-acetoin, we demonstrate that the introduction of *Cg.butA* and the use of staged genome integration with balanced gene expression enables conversion of this chassis into a stereoselective (2*S*,3*S*)-BDO producer. The resulting strain produced up to 27.9 g/L (2*S*,3*S*)-BDO in 1 L fed-batch cultivation with an overall yield of 0.20 g/g glucose and an average volumetric productivity of 0.17 g/L·h, while maintaining high enantiopurity and eliminating dependence on the spontaneous conversion of (*S*)-α-acetolactate to diacetyl.

As summarized in Table 1, this process achieves a higher titer and volumetric productivity directly from glucose than previously reported optically pure (2*S*,3*S*)-BDO processes based on engineered *L. lactis* and *E. coli*, which reached 6.7 g/L with a productivity of 0.082 g/L·h and 2.2 g/L with a productivity of 0.09 g/L/h, respectively [13, 17]. However, the overall yield of our process remains lower than that of the *L. lactis* (0.41 g/g glucose), highlighting remaining inefficiencies in carbon utilization and redox balance. This, together with the byproduct profiles observed, points to feasible routes for further improvement, including optimizing carbon and NADH flux distribution and enhancing the (*S*)-acetoin synthesis step to increase overall production efficiency. First, residual byproduct pathways continued to have a significant impact. Even after eliminating the major competing routes, considerable amounts of ethanol and glycerol were still produced. This observation indicates persistent flux through Pdc6, Adh2–5, and Gpd2, which divert pyruvate and cytosolic NADH away from (2*S*,3*S*)-BDO biosynthesis. We attempted additional deletions of *PDC6* and *GPD2*, but these modifications repeatedly failed. This is likely because the existing knockouts already impaired growth and disrupted cofactor balance, thereby reducing transformant recovery. These findings suggest that introducing further constitutive deletions is unlikely to be broadly effective. Instead, tunable, stage-specific suppression—implemented after biomass accumulation through approaches such as CRISPR interference (CRISPRi) or inducible/promoter-switch control of *PDC6*, *GPD2*, and the remaining *ADH* genes—offers a more practical strategy to restrict these byproduct pathways without compromising cell growth.

Beyond the underlying genetic basis, the fed-batch profiles show that carbon allocation is also strongly shaped by the Crabtree-positive nature of *S. cerevisiae*. Under the high-glucose conditions used here, ethanol accumulated even though the cultures were aerated, indicating overflow metabolism in which the glycolytic flux exceeds the respiratory capacity and a substantial fraction of pyruvate and NADH is therefore channeled into the fermentative ethanol pathway instead of being completely oxidized via the TCA cycle and the mitochondrial respiratory chain [40, 41]. Once cell growth had essentially ceased and glucose uptake had slowed, ethanol was gradually reassimilated while (2*S*,3*S*)-BDO continued to accumulate, suggesting that ethanol produced earlier was oxidized to acetaldehyde and acetyl-CoA and respired as the main energy and maintenance substrate, whereas residual glucose was still slowly metabolized through glycolysis and the resulting pyruvate entered the engineered (2*S*,3*S*)-BDO pathway [42, 43]. This redistribution of flux explains both the substantial contribution of the non-growing phase to the final (2*S*,3*S*)-BDO titer and the lower volumetric productivity during this period compared to the growth-associated phase.

In addition to the Crabtree effect, dissolved oxygen (DO) availability plays a central role in shaping the competition among respiratory metabolism, fermentative overflow, and (2*S*,3*S*)-BDO formation. Higher DO levels generally enhance respiratory capacity and can mitigate excessive ethanol formation, but a strongly respiratory state would also draw more pyruvate and reducing equivalents into oxidative metabolism, thereby limiting the precursor supply for (2*S*,3*S*)-BDO synthesis. Conversely, oxygen limitation promotes fermentative carbon overflow but increases ethanol accumulation, prolonging the subsequent ethanol-reassimilation period. A moderate DO level, which reduces excessive ethanol formation while avoiding excessive diversion of pyruvate into respiration, is likely to provide a more favorable balance for directing carbon toward (2*S*,3*S*)-BDO production. Process strategies such as DO-coupled feeding or DO-stat control could therefore be employed in future work to identify and maintain this optimal trade-off between ethanol suppression, respiratory activity, and (2*S*,3*S*)-BDO productivity [41, 44].

Second, the supply of the precursor (*S*)-acetoin appears to be a key rate-limiting factor. Compared with our previous (*R*)-acetoin process in the same *S. cerevisiae* background, which achieved 101.3 g/L [21], the current pathway produced markedly lower titers. Since both pathways share the upstream conversion through (*S*)-α-acetolactate, this difference most likely arises from a catalytic efficiency gap between wild-type *Bs*.AlsD and the *Bs*.AlsD^{WP} mutant. Although multi-copy integration partially alleviated this limitation, it did not fully overcome it. These findings highlight the importance of improving *Bs*.AlsD^{WP} activity and expression to enhance precursor flux toward *Cg*.ButA and thereby increase overall (2*S*,3*S*)-BDO production.

Together, this study establishes a diacetyl-independent route for (2*S*,3*S*)-BDO production in *S. cerevisiae*. Further optimization of enzyme activity, expression balance, and dynamic regulatory control will be crucial to fully harness the potential of *S. cerevisiae* as a robust and stereoselective platform for sustainable (2*S*,3*S*)-BDO biosynthesis.

5 Conclusion

This study establishes a robust *S. cerevisiae* platform capable of directly producing high-purity (2*S*,3*S*)-butanediol from glucose. By co-expressing *B. subtilis* α-acetolactate synthase (*Bs*.AlsS) and mutant α-acetolactate decarboxylase (*Bs*.AlsD^{WP}) with altered specificity toward (*S*)-acetoin formation, and introducing *C. glutamicum* L-BDH (*Cg*.ButA) for efficient and enantioselective reduction of (*S*)-acetoin,

the engineered strain produced 27.9 g/L (2*S*,3*S*)-BDO in fed-batch fermentation with high optical purity, an overall yield of 0.20 g/g glucose, and an average volumetric productivity of 0.17 g/L·h. This work provides the first demonstration of direct (2*S*,3*S*)-BDO synthesis in yeast without reliance on the spontaneous diacetyl-formation pathway and establishes *S. cerevisiae* as a versatile chassis for stereoselective diol production through precise enzyme-level pathway design.

Supplementary Information The online version contains supplementary material available at https://doi.org/10.1007/s12257-025-00255-1.

Acknowledgements This research was supported by National Research Foundation of Korea (NRF) grant funded by the Korea government (MSIT).

Author contributions S.M. Conceptualization, investigation, writing-original draft. S.C. Conceptualization, investigation, writing-original draft. M.K. Investigation, writing-original draft. C.S. Supervision. J. S.H. Conceptualization, supervision, writing-original draft, funding acquisition.

Funding Open Access funding enabled and organized by Seoul National University. Ministry of Science and ICT, South Korea, RS-2024-00335810, Seungwoo Cha, RS-2025-02214910, Ji-Sook Hahn

Data availability All data supporting the findings of this study are available from the corresponding author upon reasonable request.

Declarations

Conflict of interest The authors declare no conflict of interest.

Ethical approval Neither ethical approval nor informed consent was required for this study. Ji-Sook Hahn is an Editorial Board Member of Biotechnology and Bioprocess Engineering. Editorial Board Member status has no bearing on editorial consideration.

References

1. Richard R, Guillaume D, Jacquin M (2016) Kinetics modeling of the heterogeneously catalyzed esterification of 2,3-butanediol with acetic acid. Ind Eng Chem Res 55:5247–5256. https://doi.org/10.1021/acs.iecr.6b00133
2. Maina S, Prabhu AA, Vivek N et al (2022) Prospects on bio-based 2,3-butanediol and acetoin production: recent progress and advances. Biotechnol Adv 54:107783. https://doi.org/10.1016/j.biotechadv.2021.107783
3. Song CW, Park JM, Chung SC et al (2019) Microbial production of 2,3-butanediol for industrial applications. J Ind Microbiol Biotechnol 46:1583–1601. https://doi.org/10.1007/s10295-019-02231-0
4. Yang Z, Zhang Z (2018) Production of (2R, 3R)-2,3-butanediol using engineered *Pichia pastoris*: strain construction, characterization and fermentation. Biotechnol Biofuels 11:35. https://doi.org/10.1186/s13068-018-1031-1
5. Yan Y, Lee CC, Liao JC (2009) Enantioselective synthesis of pure (R,R)-2,3-butanediol in *Escherichia coli* with stereospecific secondary alcohol dehydrogenases. Org Biomol Chem 7:3914–3917. https://doi.org/10.1039/b913501d
6. Baek HS, Woo BY, Yoo SJ et al (2019) Antibacterial composition containing meso-2,3-butanediol. KR20160046638A, 29 April 2016
7. Li L, Wang Y, Zhang L et al (2012) Biocatalytic production of (2S,3S)-2,3-butanediol from diacetyl using whole cells of engineered *Escherichia coli*. Bioresour Technol 115:111–116. https://doi.org/10.1016/j.biortech.2011.08.097
8. Ryu CM, Lee SH, Lee HR et al (2020) Method for controlling pathogenicity of pathogenic bacteria by treating 2S,3S-Butanediol. KR102093197B1, 19 March 2020
9. Park SJ, Sohn YJ, Park SJ et al (2020) Enhanced production of 2,3-butanediol in recombinant *Escherichia coli* using response regulator DR1558 derived from *Deinococcus radiodurans*. Biotechnol Bioprocess Eng 25:45–52. https://doi.org/10.1007/s12257-019-0306-0
10. Fu J, Huo G, Feng L et al (2016) Metabolic engineering of *Bacillus subtilis* for chiral pure meso-2,3-butanediol production. Biotechnol Biofuels 9:90. https://doi.org/10.1186/s13068-016-0502-5
11. Asolkar SS, Anju M, Kumar R et al (2024) In silico screening and validation of different dehydrogenases to produce 2,3-butanediol in *Bacillus subtilis*. Biotechnol Bioprocess Eng 29:271–290. https://doi.org/10.1007/s12257-024-00053-1
12. Kou M, Cui Z, Fu J et al (2022) Metabolic engineering of *Corynebacterium glutamicum* for efficient production of optically pure (2R,3R)-2,3-butanediol. Microb Cell Fact 21:150. https://doi.org/10.1186/s12934-022-01875-5
13. Liu J, Chan SHJ, Brock-Nannestad T et al (2016) Combining metabolic engineering and biocompatible chemistry for high-yield production of homo-diacetyl and homo-(S,S)-2,3-butanediol. Metab Eng 36:57–67. https://doi.org/10.1016/j.ymben.2016.02.008
14. Faria PE, Castro AM, Freire DMG et al (2023) Enzymes and pathways in microbial production of 2,3-butanediol and 3-acetoin isomers. Crit Rev Biotechnol 43:67–81. https://doi.org/10.1080/07388551.2021.2004990
15. Li Y, Zhao X, Yao M et al (2023) Mechanism of microbial production of acetoin and 2,3-butanediol optical isomers and substrate specificity of butanediol dehydrogenase. Microb Cell Fact 22:165. https://doi.org/10.1186/s12934-023-02163-6
16. Qiu Y, Zhang J, Li L et al (2016) Engineering *Bacillus licheniformis* for the production of meso-2,3-butanediol. Biotechnol Biofuels 9:117. https://doi.org/10.1186/s13068-016-0522-1
17. Chu H, Xin B, Liu P et al (2015) Metabolic engineering of Escherichia coli for production of (2S,3S)-butane-2,3-diol from glucose. Biotechnol Biofuels 8:143. https://doi.org/10.1186/s13068-015-0324-x

18. Subramanian V, Lunin VV, Farmer SJ et al (2020) Phylogenetics-based identification and characterization of a superior 2,3-butanediol dehydrogenase for *Zymomonas mobilis* expression. Biotechnol Biofuels 13:186. https://doi.org/10.1186/s13068-020-01820-x
19. Park JM, Hong WK, Lee SM et al (2014) Identification and characterization of a short-chain acyl dehydrogenase from Klebsiella pneumoniae and its application for high-level production of L-2,3-butanediol. J Ind Microbiol Biotechnol 41:1425–1433. https://doi.org/10.1007/s10295-014-1483-7
20. Kim S, Hahn JS (2015) Efficient production of 2,3-butanediol in Saccharomyces cerevisiae by eliminating ethanol and glycerol production and redox rebalancing. Metab Eng 31:94–101. https://doi.org/10.1016/j.ymben.2015.07.006
21. Bae SJ, Kim S, Park HJ et al (2021) High-yield production of (R)-acetoin in Saccharomyces cerevisiae by deleting genes for NAD(P)H-dependent ketone reductases producing meso-2,3-butanediol and 2,3-dimethylglycerate. Metab Eng 66:68–78. https://doi.org/10.1016/j.ymben.2021.04.001
22. Cha S, Jang B, Lee D et al (2025) Efficient (S)-acetoin production in Saccharomyces cerevisiae by modulating α-acetolactate decarboxylase stereospecificity. Bioresour Technol 434:132767. https://doi.org/10.1016/j.biortech.2025.132767
23. Bae SJ, Kim S, Hahn JS (2016) Efficient production of acetoin in Saccharomyces cerevisiae by disruption of 2,3-butanediol dehydrogenase and expression of NADH oxidase. Sci Rep 6:27667. https://doi.org/10.1038/srep27667
24. Baek SH, Kwon EY, Bae SJ et al (2017) Improvement of d-lactic acid production in Saccharomyces cerevisiae under acidic conditions by evolutionary and rational metabolic engineering. Biotechnol J 12:1700015. https://doi.org/10.1002/biot.201700015
25. Baek SH, Kwon EY, Kim YH et al (2016) Metabolic engineering and adaptive evolution for efficient production of D-lactic acid in Saccharomyces cerevisiae. Appl Microbiol Biotechnol 100:2737–2748. https://doi.org/10.1007/s00253-015-7174-0
26. González E, Fernández MR, Larroy C et al (2000) Characterization of a (2R,3R)-2,3-butanediol dehydrogenase as the Saccharomyces cerevisiae YAL060W gene product. Disruption and induction of the gene. J Biol Chem 275:35876–35885. https://doi.org/10.1074/jbc.M003035200
27. Bruni GO, Terrell E (2022) A review on the production of C4 platform chemicals from biochemical conversion of sugar crop processing products and by-products. Fermentation 8:216. https://doi.org/10.3390/fermentation8050216
28. González E, Fernández MR, Marco D et al (2010) Role of Saccharomyces cerevisiae oxidoreductases Bdh1p and Ara1p in the metabolism of acetoin and 2,3-butanediol. Appl Environ Microbiol 76:670–679. https://doi.org/10.1128/AEM.01521-09
29. Mumberg D, Müller R, Funk M (1995) Yeast vectors for the controlled expression of heterologous proteins in different genetic backgrounds. Gene 156:119–122. https://doi.org/10.1016/0378-1119(95)00037-7
30. Eberhardt J, Santos-Martins D, Tillack AF et al (2021) AutoDock Vina 1.2.0: new docking methods, expanded force field, and python bindings. J Chem Inf Model 61:3891–3898. https://doi.org/10.1021/acs.jcim.1c00203
31. Trott O, Olson AJ (2010) AutoDock Vina: improving the speed and accuracy of docking with a new scoring function, efficient optimization, and multithreading. J Comput Chem 31:455–461. https://doi.org/10.1002/jcc.21334
32. Otagiri M, Ui S, Takusagawa Y et al (2010) Structural basis for chiral substrate recognition by two 2,3-butanediol dehydrogenases. FEBS Lett 584:219–223. https://doi.org/10.1016/j.febslet.2009.11.068
33. Otagiri M, Kurisu G, Ui S et al (2001) Crystal structure of meso-2,3-butanediol dehydrogenase in a complex with NAD+ and inhibitor mercaptoethanol at 1.7 A resolution for understanding of chiral substrate recognition mechanisms. J Biochem 129:205–208. https://doi.org/10.1093/oxfordjournals.jbchem.a002845
34. Pettersen EF, Goddard TD, Huang CC et al (2004) UCSF chimera–a visualization system for exploratory research and analysis. J Comput Chem 25:1605–1612. https://doi.org/10.1002/jcc.20084
35. Cha J, Lim CH, Lee J et al (2024) Algal biomass-based zero-waste biorefinery for producing optically pure (R)-γ-valerolactone and carbonaceous electrodes applicable for energy storage devices. Chem Eng J 490:151713. https://doi.org/10.1016/j.cej.2024.151713
36. Radoš D, Turner DL, Catarino T et al (2016) Stereospecificity of *Corynebacterium glutamicum* 2,3-butanediol dehydrogenase and implications for the stereochemical purity of bioproduced 2,3-butanediol. Appl Microbiol Biotechnol 100:10573–10583. https://doi.org/10.1007/s00253-016-7860-6
37. Wang Z, Song Q, Yu M et al (2014) Characterization of a stereospecific acetoin(diacetyl) reductase from *Rhodococcus erythropolis* WZ010 and its application for the synthesis of (2S,3S)-2,3-butanediol. Appl Microbiol Biotechnol 98:641–650. https://doi.org/10.1007/s00253-013-4870-5
38. Park SH, Hahn JS (2019) Development of an efficient cytosolic isobutanol production pathway in *Saccharomyces cerevisiae* by optimizing copy numbers and expression of the pathway genes based on the toxic effect of α-acetolactate. Sci Rep 9:3996. https://doi.org/10.1038/s41598-019-40631-5
39. van Bergen B, Cyr N, Strasser R et al (2016) A,β-dicarbonyl reduction is mediated by the Saccharomyces Old Yellow Enzyme. FEMS Yeast Res 16:fow059. https://doi.org/10.1093/femsyr/fow059
40. Hagman A, Piškur J (2015) A study on the fundamental mechanism and the evolutionary driving forces behind aerobic fermentation in yeast. PLoS ONE 10:e0116942. https://doi.org/10.1371/journal.pone.0116942
41. Habegger L, Rodrigues Crespo K, Dabros M (2018) Preventing overflow metabolism in crabtree-positive microorganisms through on-line monitoring and control of fed-batch fermentations. Fermentation 4:79. https://doi.org/10.3390/fermentation4030079
42. de Smidt O, du Preez JC, Albertyn J (2012) Molecular and physiological aspects of alcohol dehydrogenases in the ethanol metabolism of *Saccharomyces cerevisiae*. FEMS Yeast Res 12:33–47. https://doi.org/10.1111/j.1567-1364.2011.00760.x
43. Orlandi I, Ronzulli R, Casatta N et al (2013) Ethanol and acetate acting as carbon/energy sources negatively affect yeast chronological aging. Oxid Med Cell Longev 2013:802870. https://doi.org/10.1155/2013/802870
44. Yang FC, Maa DW (1998) Fed-batch culture of yeast *Saccharomyces cerevisiae* with a DO-stat method by a fuzzy controller. Bioprocess Eng 18:79–82. https://doi.org/10.1007/PL00008980